Analyst

PAPER

View Article Online
View Journal | View Issue

Cite this: *Analyst*, 2018, **143**, 4459

Precursor ion survival energies of protonated *N*-glycopeptides and their weak dependencies on high mannose *N*-glycan composition in collision-induced dissociation†

Forouzan Aboufazeli and Eric D. Dodds *

Fully realizing the capabilities of tandem mass spectrometry (MS/MS) for analysis of glycosylated peptides will require further understanding of the unimolecular dissociation chemistry that dictates their fragmentation pathways. In this context, the overall composition of a given glycopeptide ion is a key characteristic; however, the extent to which the carbohydrate moiety influences the preferred dissociation channels has received relatively little study. Here, the effect of glycan composition on energy-resolved collision-induced dissociation (CID) behavior was studied for a select menu of 30 protonated high mannose type N-linked glycopeptide ions. Groups of analytes which shared a common charge state, polypeptide sequence, and glycosylation site exhibited 50% precursor ion survival energies that varied only slightly as the size and composition of the oligosaccharide was varied. This was found to be true regardless of whether the precursor ion survival energies were normalized for the number of available vibrational degrees of freedom. The practical consequence of this was that a given collision energy brought about highly similar levels of precursor ion depletion and structural information despite systematic variation of the glycan identity. This lack of sensitivity to oligosaccharide composition stands in contrast to other physicochemical properties of glycopeptide ions (*e.g.*, polypeptide composition, charge state, charge carrier) which sharply influence their energy-resolved CID characteristics. On the whole, these findings imply that the deliberate selection of CID energies to bring about a desired range of fragmentation pathways does not necessarily hinge on the nature of the glycan.

Received 3rd May 2018,
Accepted 21st August 2018

DOI: 10.1039/c8an00830b

rsc.li/analyst

Introduction

The ubiquitous, enzymatically-catalyzed, and non-template-driven modification of proteins by carbohydrates is essential to a multitude of fundamental life processes.[1–4] Consequently, the glycosylation status of proteins has garnered significant attention from the standpoint of human health and disease.[5–7] In this context, anomalous modes of protein glycosylation may be predictive or indicative of a given disease state, as well documented in many forms of cancer.[8–10] Alternatively, defects of protein glycosylation may serve to trigger a given disease state, such as in the various congenital disorders of glycosylation.[11–14] Furthermore, while protein-linked oligosaccharides have been widely recognized for some time as focal points of intermolecular recognition,[15,16] protein-borne glycans have also become increasingly credited for their roles in biomolecular signaling.[17,18] Taken together, these considerations have served to stimulate great interest in the area of biomedical glycoproteomics. Nevertheless, the determination of glycosylation profiles across many proteins in samples of realistic biological complexity lies well outside of the routine, remaining solidly in the purview of specialized research.

Mass spectrometry (MS) provides an already powerful yet still actively maturing methodological platform for probing the structures of glycoproteins.[19–24] MS-based glycoprotein characterization is often performed following enzymatic degradation such that the glycan topology, sites of glycosylation, and site heterogeneity can be inferred through analysis of the resultant proteolytic glycopeptides.[25–28] Although the accurately measured monoisotopic masses of glycopeptides can, in some cases, be used to make putative glycopeptide assignments,[29,30] further verification of glycopeptide composition and connectivity are usually carried out based on tandem MS (MS/MS) analyses.[31,32] There exist many available modes of ion dissociation for this purpose,[33–36] with the majority of these having been extensively applied to the MS/MS analysis of glyco-

Department of Chemistry, University of Nebraska – Lincoln, Lincoln, NE, 68588-0304, USA. E-mail: eric.dodds@unl.edu; Tel: +1.402.472.3592

†Electronic supplementary information (ESI) available: Compositions, charge states (z), degrees of freedom (f_v), and 50% precursor ion survival data (ΔU_{50}, E_{k50}, and E_{n50}) for all glycopeptide ions studied. See DOI: 10.1039/c8an00830b

peptides.[31,32] This includes methods based on ion-neutral collisions, such as in collision-induced dissociation (CID);[37,38] methods based on ion/electron or ion/ion charge recombination, such as electron capture dissociation (ECD) or electron transfer dissociation (ETD);[39–44] and methods based on absorption of photons, such as infrared multiphoton dissociation (IRMPD) and ultraviolet photodissociation (UVPD).[45–50]

Unsurprisingly, the widely varying energy regimes, activation timescales, and activation mechanisms encompassed by this assortment of MS/MS methods are reflected accordingly in the outcomes of the MS/MS experiments. Indeed, some of these methods have been demonstrated to provide very different coverages of glycopeptide topology relative to one another, providing the opportunity to collect highly orthogonal information by invoking multiple types of MS/MS fragmentation. A particularly potent combination has been that of CID and ETD, which for protonated glycopeptide ions tend to provide information on the oligosaccharide connectivity and polypeptide sequence, respectively.[31,32] A number of approaches have been developed to combine these two MS/MS methods such that the advantages of both are afforded for glycopeptide analysis.[51–55] Nevertheless, any strategy that relies solely on ETD to obtain peptide sequence information is inherently subject to the limitations of ETD, including low precursor ion to fragment ion conversion efficiency for glycopeptides, particularly at lower charge states.[56,57]

The less frequently appreciated capability of CID to yield polypeptide sequence information provides an alternative avenue to the determination of covalent relationships between both monosaccharide and amino acid residues of glycopeptide ions. This is possible because CID is self-complementary in the context of glycopeptide MS/MS analysis, with the type of information garnered depending on the selected collision energy.[58,59] This raises the question of whether the optimum MS/MS method for obtaining peptide sequence information (*i.e.*, CID or ETD) depends on the physical and chemical characteristics of the specific glycopeptide ion of interest. In concert, these factors have prompted significant interest in elucidating how the properties of glycopeptides ions dictate their dissociation channels, and how experimental and instrumental parameters can be tuned to deliberately gather a desired type of glycopeptide structural information.

Motivated by the considerations described above and inspired by previous observations on the ability of CID to capture both peptide sequence and glycan connectivity in a collision energy dependent manner,[60–67] we have developed a significant interest in the energy-resolved CID behavior of glycopeptide ions. Previously, we demonstrated that oligosaccharide and polypeptide fragmentation could be accessed for a wide variety of glycopeptide ions, and that alternating between optimum collision energies for each type of scission allowed the collection of aggregate spectra covering most of the glycopeptide connectivity.[58] An obstacle towards the generalized and automated application of this approach was also realized, in that the collision energies yielding useful information on either the glycan or peptide moieties were strikingly different for the various precursor ions studied. In order to address this issue, we further studied a family of closely related model glycopeptides in which the peptide composition and charge state were varied while holding the identity of the glycan constant. This work revealed that the relative proton mobility[68,69] of the various glycopeptides was a decisive factor in determining the collision energies providing glycan connectivity information. By contrast, the collision energies providing peptide fragmentation information exhibited essentially no correlation with the precursor ion proton mobility, but instead were better explained by the proton mobility of intermediate fragmentation products appearing prior to the onset of peptide backbone scission.[59] We have also compared the energy-resolved CID characteristics of doubly protonated, doubly sodiated, and hybrid protonated sodium adduct glycopeptide ions (all doubly charged) where again the peptide composition and sequence were varied while fixing the identity of the glycan. These studies uncovered marked differences in the stabilities of precursor ions with these different charge carriers, with those involving sodiation having more similar precursor ion survival energies as the amino acid composition and sequence were varied.[70]

The present study was undertaken to address one of the parameters that has not been systematically varied in previous studies of glycopeptide energy-resolved CID: namely, the composition and size of the attached glycan. Precursor ion survival curves were measured for an assemblage of protonated glycopeptide ions encompassing four high mannose N-linked oligosaccharide compositions, four peptide backbone sequences, and three charge states. As in previous works, the findings of this study verify the heavy influence of proton mobility (and, relatedly, amino acid composition and ion charge state) on the 50% precursor ion survival energies of protonated glycopeptide ions. Contrastingly, elongation of the *N*-glycan was not found to have a significant impact on the dissociation thresholds of the same ions. Moreover, when the 50% precursor ion survival energies were normalized for the number of available vibrational degrees of freedom, the influence of the *N*-glycan size and composition was often further minimized. These findings suggest that, for high mannose *N*-glycopeptides, the identity of the glycan is not a significant factor in determining the absolute collision energies that lead to a given level of precursor ion depletion, or furnish a given type of structural information. This result is encouraging in the context of large-scale glycoproteomics, as this implies that the identity of the glycan may not play a major role in the rational selection of collision energies for glycopeptide analysis.

Experimental

Glycopeptide preparation

Bovine ribonuclease B (RNase B), urea, dithiothreitol, iodoacetamide, imidazole, formic acid, and trypsin were acquired from Sigma-Aldrich (St Louis, MO, USA). HPLC grade acetonitrile was purchased from Fisher Scientific (Fair Lawn, NJ,

USA). HPLC grade water was obtained from Burdick & Jackson (Muskegon, MI, USA). A solution of 10 μg μL^{-1} of RNase B in 8 M urea and 50 mM NH_4HCO_3 (pH 7.5) was prepared to provide a stock solution of the denatured glycoprotein. Disulfide linkages were reduced by addition of 10 μL of 450 mM dithiothreitol in 50 mM NH_4HCO_3 buffer (pH 7.5) with incubation for 1 h in a 55 °C water bath, and the free cysteine side chains were then alkylated by treatment with 10 μL of 500 mM iodoacetamide in 50 mM NH_4HCO_3 (pH 7.5) with incubation in the dark at room temperature. The sample was next diluted with 175 μL of 50 mM NH_4HCO_3 (pH 7.5), mixed thoroughly by vortexing, treated with 0.5 μg μL^{-1} trypsin, and held at 37 °C in a gravity convection incubator for 12–16 hours. Next, the volume of the mixture was reduced to approximately 10 μL *via* vacuum centrifugation. The resulting concentrate was reconstituted with 100 μL of 80% CH_3CN/0.1% HCOOH, and this solution was divided into 20 μL aliquots for further workup. Glycopeptides were purified and enriched from the tryptic digest by solid phase extraction (SPE) using a zwitterionic hydrophilic interaction liquid chromatography (ZIC HILIC) micropipette tips obtained from Protea (Somerset, NJ, USA). SPE was carried out by first conditioning the stationary phase with water, equilibrating with 80% CH_3CN/0.1% HCOOH, then loading an aliquot of glycopeptide digest. Next, the tip was washed using 80% CH_3CN/0.1% HCOOH, followed by elution with 0.1% formic acid. In some cases, 10 μL of 10 μg μL^{-1} imidazole was added to the enriched glycopeptide preparation in order to increase the abundance of lower charge state ions for study.

Tandem mass spectrometry

Corning Pyrex borosilicate capillary tubes with a 1.5–1.8 mm inner diameter and a length of 100 mm (Corning, NY, USA) were purchased from Fisher Scientific, and were used to fabricate emitters for nanoelectrospray ionization (nESI) with the aid of a vertical micropipette puller. Purified glycopeptide solutions were loaded into the homemade borosilicate emitters and placed in contact with a platinum wire (Alfa Aesar; Ward Hill, MA, USA) that served to apply the potential difference necessary for nESI. All MS/MS experiments were accomplished through the use of a Synapt G2-S HDMS quadrupole time-of-flight (Q-TOF) hybrid mass spectrometer (Waters; Manchester, UK). The nESI capillary voltage was optimized for each experiment, and ranged from 1.0–1.5 kV. The trapping region stacked ring ion guide of the instrument was used as the collision cell for MS/MS *via* CID, where argon served as the collision gas at a pressure of approximately 5.0×10^{-3} mbar. The applied potential difference through which ions were accelerated into the collision cell (ΔU) was varied over the range of 0–75 V in 5 V increments to collect energy-resolved CID data.

Data handling

MS/MS spectra were acquired and processed using MassLynx 4.1 (Waters). Additional data analysis, processing, and graphing was accomplished using SigmaPlot 10.1 (Systat; Chicago, IL, USA) and IGOR Pro 6.3 (WaveMetrics; Lake Oswego, OR, USA). Integrated peak areas were calculated for precursor and fragment ions appearing in MS/MS spectra using a custom script written and implemented in IGOR Pro 6.3. Fragmentation products resulting from scission of the oligosaccharide were assigned using Domon/Costello nomenclature where possible;[71] however, if a given product ion might have arisen from multiple potential fragmentation pathways (thus rendering the specific Domon/Costello cleavage type ambiguous), compositional assignments were made by indicating the observed monosaccharide loss or losses. In the latter of these conventions, the monosaccharides *N*-acetylglucosamine and mannose were abbreviated as GlcNAc and Man, respectively. Roepstorff/Fohlmann nomenclature was used to assign fragmentation products resulting from scission of the peptide backbone.[72] The symbols proposed by Varki *et al.* were used to diagram *N*-glycan structures.[73,74] Underlining was used in order to indicate the site of glycosylation on a given peptide sequence.

Results

Overview

The glycopeptides studied here were generated by tryptic digestion of RNase B, a well characterized model glycoprotein with heterogeneous, high mannose type *N*-glycosylation at a single site. In addition, the site of glycosylation is flanked by several potential tryptic cleavage sites (*i.e.*, C-terminal of arginine and lysine residues). This facilitates the production of a heterogeneous population of tryptic cleavage products, as steric interference imposed by the oligosaccharide chain decreases the rate of proteolysis at adjacent cleavage sites.[75–78] As a result, a combination of fully tryptic and various partially tryptic peptide backbones was generated, providing glycopeptides with amino acid sequences of NLTK, NLTKDR, SRNLTK, and SRNLTKDR. Each of these peptide groups were studied in their glycosylated forms, with the *N*-oligosaccharides $GlcNAc_2Man_5$, $GlcNAc_2Man_6$, $GlcNAc_2Man_7$, and $GlcNAc_2Man_8$. The $GlcNAc_2Man_9$ glycoform of RNase B was not included in these experiments, as this is the least abundant glycoform and did not yield sufficient ion signal to be studied reproducibly across glycopeptides with different amino acid sequences and charge states. Upon nESI-Q-TOF-MS analysis, each glycopeptide of interest was observed in two charge states, including $z = 1$ (*i.e.*, $[M + H]^+$), $z = 2$ (*i.e.*, $[M + 2H]^{2+}$), and $z = 3$ (*i.e.*, $[M + 3H]^{3+}$). The various glycopeptide ions studied here are graphically summarized in Fig. 1. We note here that the $[NLTK + GlcNAc_2Man_7 + H]^+$ and $[NLTK + GlcNAc_2Man_8 + H]^+$ ions were not included in these experiments due to insufficient ion signal for reproducible study.

Precursor ion survival curves

Each glycopeptide ion targeted for study was quadrupole selected and subjected to CID with a range of collision energies (*i.e.*, ΔU values). In each case, the integrated peak area of the precursor ion was measured relative to the total

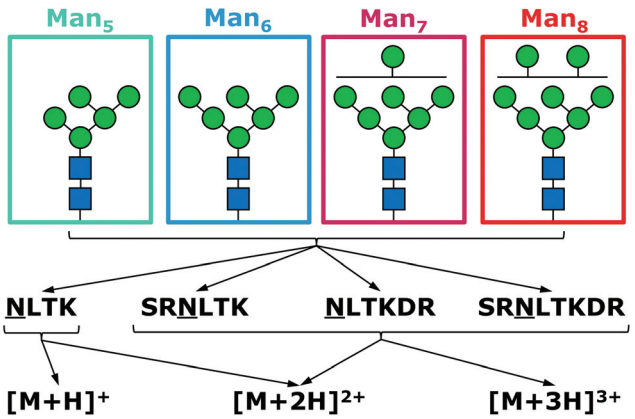

Fig. 1 Illustrated summary of the protonated high mannose N-linked glycopeptide ions studied here. The suite of analytes encompassed *N*-glycans with the compositions $GlcNAc_2Man_5$, $GlcNAc_2Man_6$, $GlcNAc_2Man_7$, and $GlcNAc_2Man_8$; peptides with the sequences NLTK, SRNLTK, NLTKDR, and SRNLTKDR; and charge states ranging from $z = +1$ to $z = +3$.

integrated peak area of the spectrum, expressed as a percentage, and plotted as a function of collision energy. The results shown in Fig. 2 demonstrate that glycopeptides having the same amino acid sequence and charge state (*i.e.*, glycopeptides that differ only in the identity of the glycan) tend to exhibit precursor ion survival curves that are grouped over a relatively narrow range of ΔU values. For example, as illustrated in Fig. 2a, the doubly protonated ions corresponding to the glycoforms of NLTK exhibit highly overlapping precursor ion survival curves, with all of their 50% depletion points occurring within approximately 1 V of one another. For the same glycopeptides in their singly charged forms, the precursor ion survival curves are shifted to significantly higher collision energies. This is due to two combined effects: (1) the singly charged precursor ions are imparted with only half the kinetic energy of their doubly charged counterparts when accelerated through a given potential difference; and (2) the proton mobilities[68,69] of the NLTK glycoforms are significantly lower for the singly charged precursors as compared to the doubly charged precursors, thus increasing the activation barriers that must be surmounted in order to access charge directed fragmentation mechanisms.[79] Despite the higher collision energies required

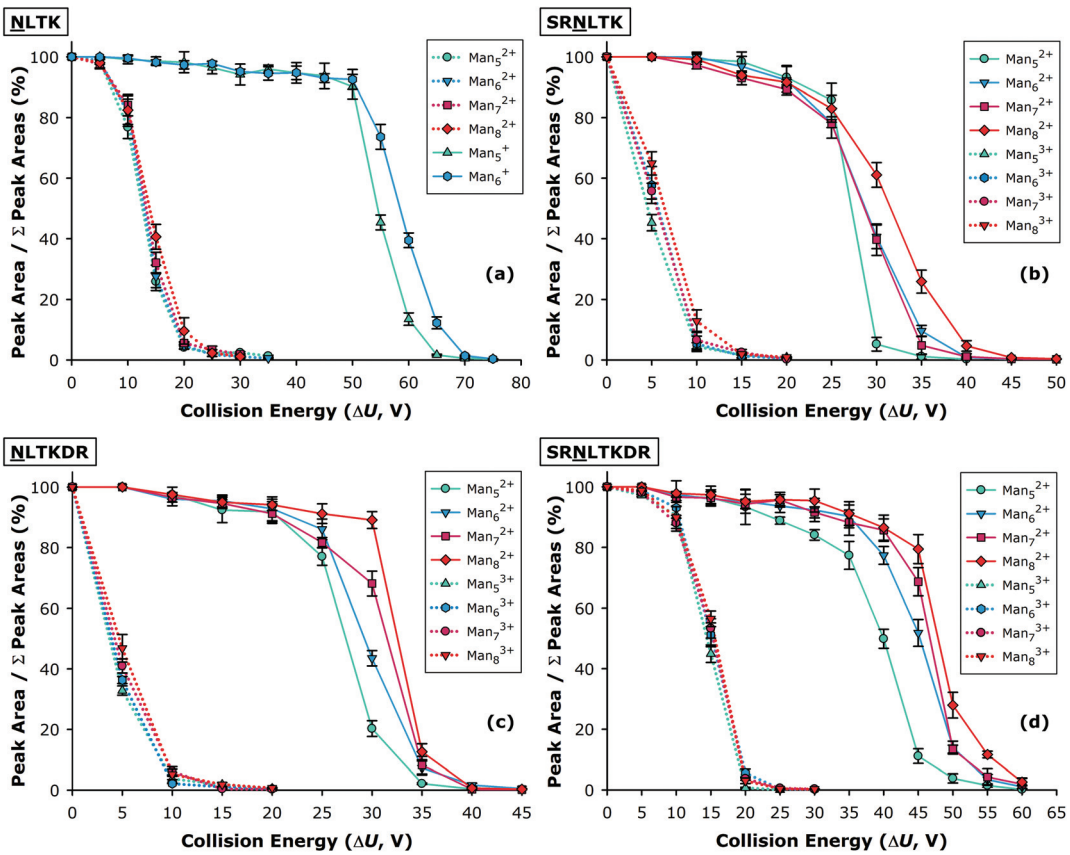

Fig. 2 Precursor ion survival curves for glycopeptides with the peptide sequences NLTK (a), SRNLTK (b), NLTKDR (c), and SRNLTKDR (d), harboring N-linked glycans with the compositions $GlcNAc_2Man_5$, $GlcNAc_2Man_6$, $GlcNAc_2Man_7$, and $GlcNAc_2Man_8$. Two charge states were considered in each case: $z = 1$ and $z = 2$ in (a); $z = 2$ and $z = 3$ in (b–d). Error bars represent the standard deviation of four replicate determinations arising from separate acquisitions. Data for the $[NLTK + GlcNAc_2Man_7 + H]^+$ and $[NLTK + GlcNAc_2Man_8 + H]^+$ ions are not shown in (a) due to insufficient ion signal for reproducible study.

to deplete the singly charged precursor ions, their survival curves remained heavily overlapped, reaching 50% depletion within 4 V of one another. This is a rather narrow range in comparison to the shifts in precursor ion survival induced by changes in charge state and proton mobility, which in this example amounted to an approximately 45 V shift in the position of the precursor ion survival curves.

The same measurements were performed for the four high mannose glycoforms of SRNLTK, NLTKDR, and SRNLTKDR in their $[M + 2H]^{2+}$ and $[M + 3H]^{3+}$ ionic forms (Fig. 2b–d). These energy-resolved CID results reinforce the qualitative conclusions reached in the discussion of Fig. 2a above, in that the precursor ion survival curves exhibited only modest shifts as a result of increasing the number of mannose residues. By contrast, the dissociation thresholds for the same glycopeptides were subject to much larger shifts with alterations in charge state and proton mobility. Nevertheless, some trending toward increased precursor ion stability was apparent as the number of mannose residues increased. This prompted the question of whether these shifts in precursor ion stability were related to some change in the underlying chemistry of dissociation, or whether this was simply a degrees of freedom effect (*i.e.*, greater stability upon vibrational activation arising from an increase in the number of available normal modes).[80,81] This question was addressed by the analyses described in the succeeding section.

Precursor ion survival energies

In order to more quantitatively compare the stabilities of the glycopeptide ions under examination, the collision energies required to achieve half depletion of the precursor ion were determined. This was done by least squares fitting of the approximately linear portions of the precursor ion survival curves presented in Fig. 2, and subsequent calculation of the collision energies that brought about precursor ion survivals of 50% (ΔU_{50}). The corresponding initial ion kinetic energies that resulted in 50% precursor ion survivals (E_{k50}) were then calculated according to eqn (1), where z represents the integer charge state of the ion:

$$E_{k50} = z\Delta U_{50}. \quad (1)$$

The number of vibrational degrees of freedom (f_v) was also calculated for each glycopeptide of interest

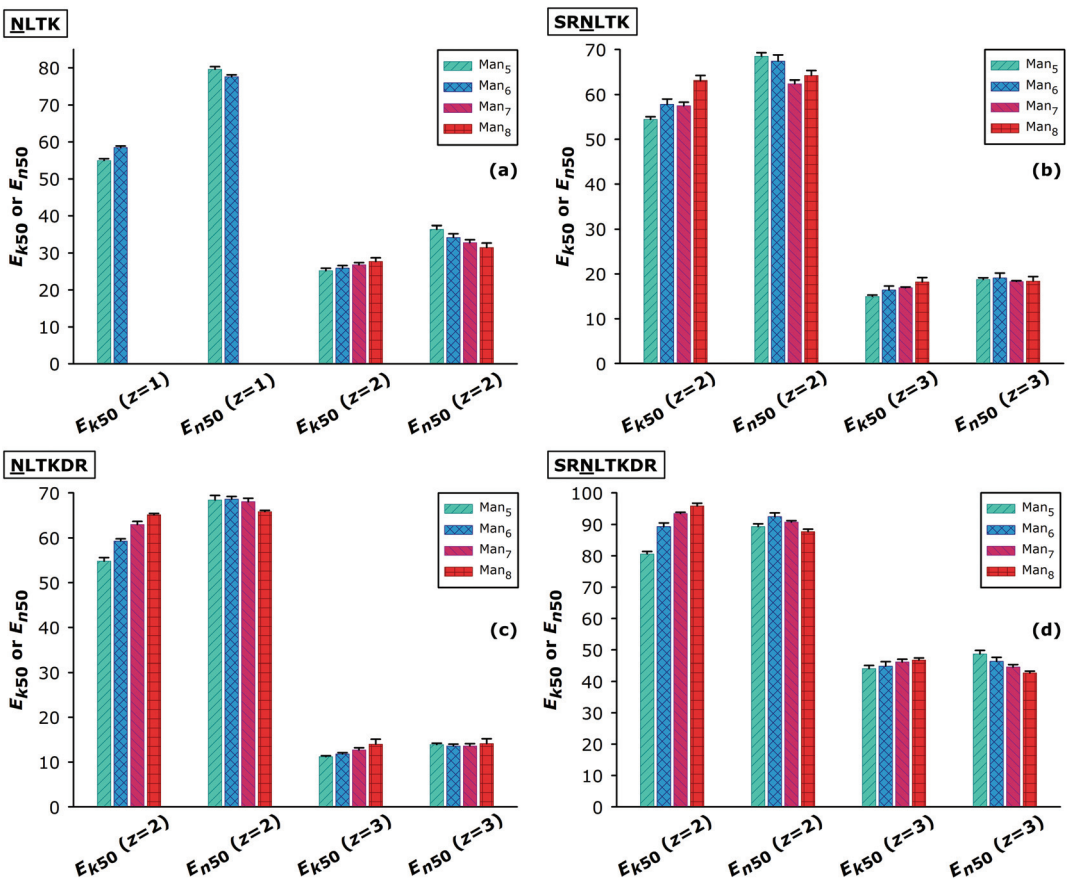

Fig. 3 Precursor ion survival energies (expressed as both E_{k50} and E_{n50} values) for glycopeptides with the peptide sequences NLTK (a), SRNLTK (b), NLTKDR (c), and SRNLTKDR (d), harboring N-linked glycans with the compositions $GlcNAc_2Man_5$, $GlcNAc_2Man_6$, $GlcNAc_2Man_7$, and $GlcNAc_2Man_8$. Two charge states were considered in each case: $z = 1$ and $z = 2$ in (a); $z = 2$ and $z = 3$ in (b–d). Error bars represent the standard deviation of four replicate determinations arising from separate acquisitions. Data for the $[NLTK + GlcNAc_2Man_7 + H]^+$ and $[NLTK + GlcNAc_2Man_8 + H]^+$ ions are not shown in (a) due to insufficient ion signal for reproducible study.

using eqn (2), where n indicates the number of atoms:

$$f_v = 3n - 6. \quad (2)$$

Finally, the E_{k50} and f_v values were used to calculate the degrees of freedom normalized 50% precursor ion survival energy (E_{n50}), as provided by eqn (3):

$$E_{n50} = \frac{10^3 E_{k50}}{f_v} = \frac{10^3 z \Delta U_{50}}{3n - 6}. \quad (3)$$

This relation includes a factor of 10^3 so that the E_{n50} values scale conveniently for comparison to the corresponding ΔU_{50} values. Conceptually, E_{n50} represents the initial precursor ion kinetic energy per vibrational mode which reduced the initial precursor ion population to one-half of the total integrated peak area of the CID spectrum. Because this metric accounts for the number of vibrational modes, differences in precursor ion stability arising from the so-called "degrees of freedom effect" are effectively compensated for.[80,81] All relevant f_v, ΔU_{50}, E_{k50}, and E_{n50} values have been provided in Table S1 of the ESI.†

A comparison of E_{k50} and E_{n50} values for the glycopeptide ions under study is presented in Fig. 3. Overall, the 50% precursor ion survival energies exhibited only a weak dependence on the composition of the *N*-glycan when varied from $GlcNAc_2Man_5$ to $GlcNAc_2Man_8$. This was found to be the case regardless of whether these energies were normalized for the available degrees of vibrational freedom. When the glycan composition was varied while holding the polypeptide sequence and charge state constant, the E_{n50} values were generally found to occupy a comparable or narrower range of values as compared to the E_{k50} values. For example, as seen in Fig. 3d, the E_{k50} values for the $[SRNLTKDR + GlcNAc_2Man_{5-8} + 2H]^{2+}$ glycopeptides ranged from 80.6 ± 0.8 to 95.8 ± 0.9 (a change of about 19%), with the values steadily increasing as

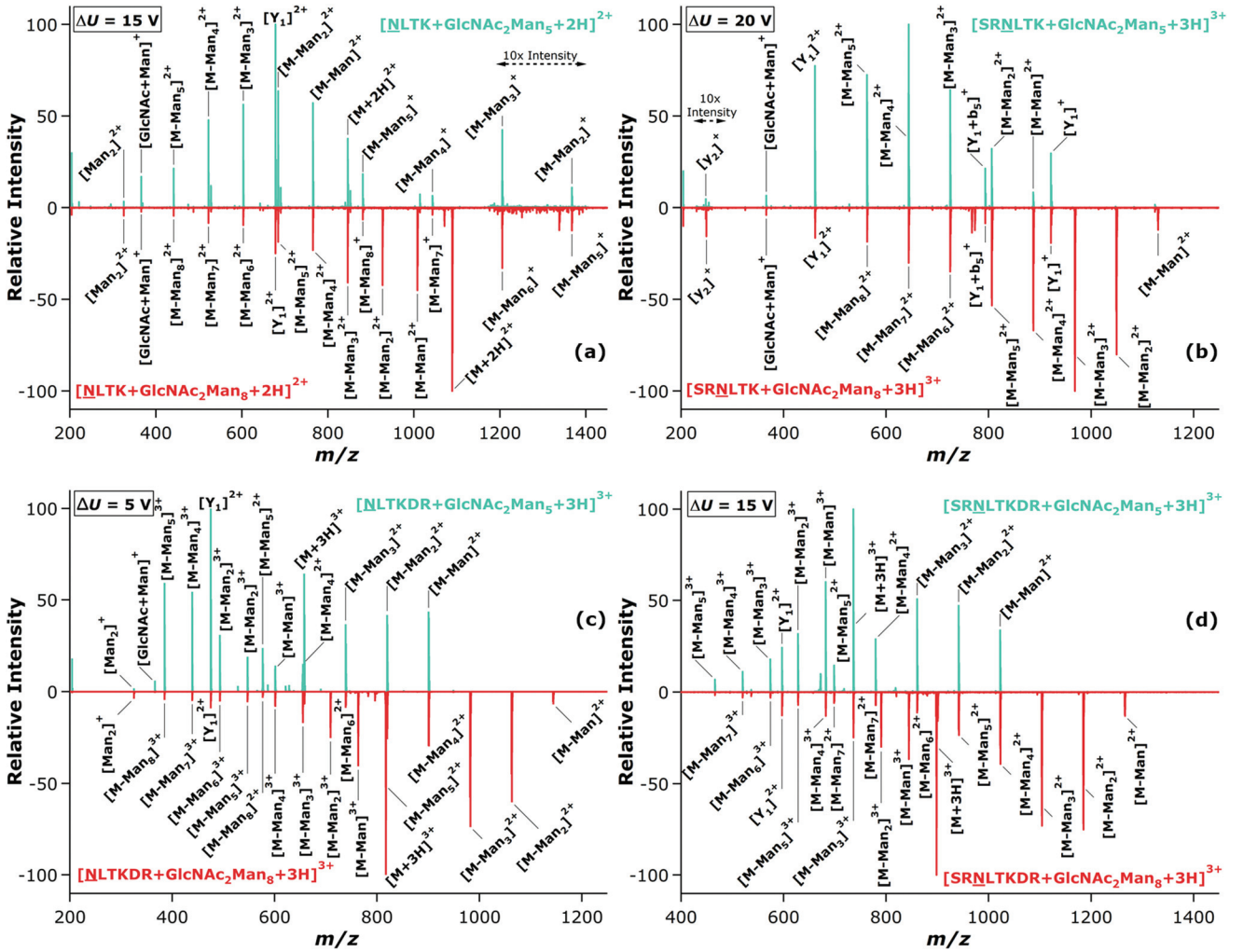

Fig. 4 CID spectra for glycopeptides with the peptide sequences NLTK (a), SRNLTK (b), NLTKDR (c), and SRNLTKDR (d), harboring N-linked glycans with the compositions $GlcNAc_2Man_5$ (top, upright traces) and $GlcNAc_2Man_8$ (bottom, inverse traces). For each comparison, the same ΔU (indicated in each inset) was applied to acquire the two fragmentation spectra.

with the addition of each successive mannose residue. Meanwhile, the E_{n50} values for the same glycopeptide ions ranged from 87.7 ± 0.8 to 92.4 ± 1.2 (a change of about 5%) and exhibited no clear dependence on the number of mannose residues. This general behavior was also observed for other groups of glycopeptides, which followed qualitatively similar relationships between glycan composition and precursor ion survival energies (*e.g.*, Fig. 3b for the z = 3 ions; Fig. 3c for the z = 2 and z = 3 ions). In other cases, addition of mannose residues was found to bring about small decreases in E_{n50} values despite concomitant increases in the E_{k50} metric (*e.g.*, Fig. 3a for the z = 1 and z = 2 ions; Fig. 3b for the z = 2 ions; Fig. 3d for the z = 3 ions). In all cases, changes in the composition of the attached high mannose *N*-glycan had only a modest impact on the precursor ion stabilities when compared to the far more influential characteristics of charge state and amino acid composition.

Assessment of collision energy matched spectra

A comparison of the dissociation spectra for the various $GlcNAc_2Man_5$ and $GlcNAc_2Man_8$ glycopeptides was next conducted with the collision energies held constant for these two glycoforms of each peptide under examination. In this way, the structural information provided on each analyte could be evaluated for cases in which no attempt was made to adjust CID conditions according to the size of the *N*-glycan borne by the glycopeptide. In Fig. 4, the collision energy matched CID spectra for the doubly protonated NLTK glycoforms and the triply protonated SRNLTK, NLTKDR, and SRNLTKDR glycoforms are plotted with the spectra for the $GlcNAc_2Man_5$ glycopeptides shown as upright traces and the $GlcNAc_2Man_8$ glycopeptides shown as inverted traces for comparison. In each case, the collision energies were selected to provide CID spectra that had the qualitative appearance of containing

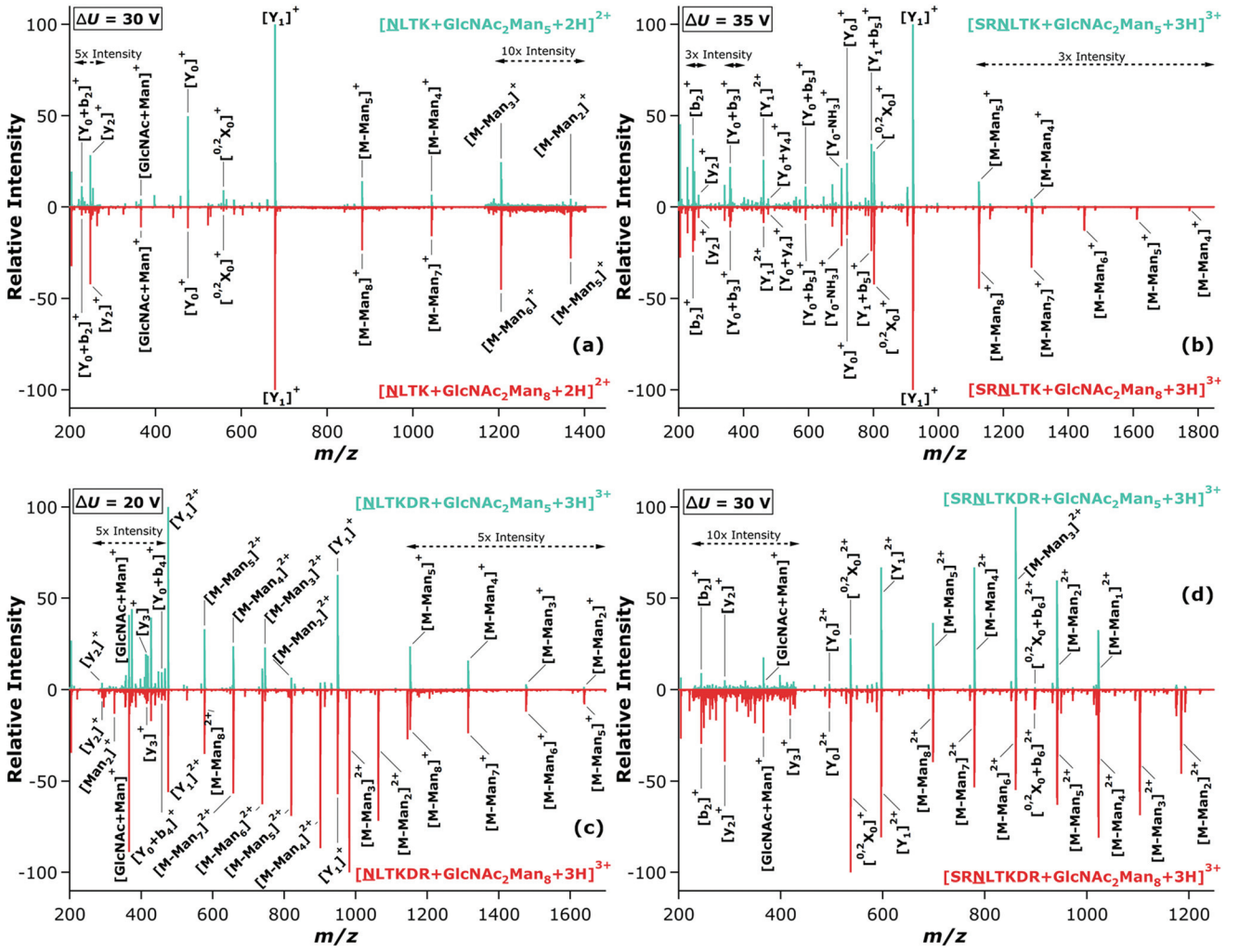

Fig. 5 CID spectra for glycopeptides with the peptide sequences NLTK (a), SRNLTK (b), NLTKDR (c), and SRNLTKDR (d), harboring N-linked glycans with the compositions $GlcNAc_2Man_5$ (top, upright traces) and $GlcNAc_2Man_8$ (bottom, inverse traces). For each comparison, the same ΔU (indicated in each inset) was applied to acquire the two fragmentation spectra. The collision energies were selected such that the applied ΔU values were 15 V greater than those shown in Fig. 4.

numerous structurally informative fragment ions; nevertheless, as noted above, each pairwise comparison of the two glycoforms was conducted at the same ΔU. In general, these fragmentation spectra were dominated by Y-type cleavages of the *N*-glycan, leading to an assortment of [M-Man$_i$] product ions and ultimately resulting in loss of all mannose residues. In each case, the Y_1 ion was also prominently observed. In some cases, additional dissociation pathways were noted, including B-type fragmentation oligosaccharide as evidenced by the presence of oxonium ions (*e.g.*, the $[Man_2]^+$ ion seen in Fig. 4a and c) and scission of the peptide backbone (*e.g.*, the y_2 and b_5 cleavages seen in Fig. 4b). Strikingly, the fragment ions produced yielded by each glycoform at the same collision energy were heavily overlapped, yielding essentially the same compositional and structural information. In fact, the only ions not appearing in the spectra of both glycoforms were the residual precursor ion, if present, and the larger monosaccharide loss fragments possible for the $GlcNAc_2Man_8$ ions, but not the $GlcNAc_2Man_5$ ions. As shown in Fig. 5, the same qualitative behavior, characterized by heavily overlapped fragmentation spectra for glycoforms, was also observed when the comparisons were repeated with all ΔU values being increased by 15 V. In these more energetic CID experiments, distinctly different fragment ion populations were observed. These dissociation products tended to include increased representation of peptide backbone cleavages (as seen in all the examples presented in Fig. 5a–d) as well as cross-ring cleavage of the *N*-glycan (*e.g.*, the $^{0,2}X_0$ fragments seen in Fig. 5a, b and d). Nevertheless, these collision energy matched spectra remained remarkably similar in terms of the fragment ions yielded and the information they provided. This illustrates that the high correlation between the CID spectra of $GlcNAc_2Man_5$ and $GlcNAc_2Man_8$ glycoforms is not unique to a certain set of CID conditions but exists over a significant range of ΔU values, including those corresponding to quite different levels of precursor ion depletion. On the whole, these findings are consistent with the previous results focused on precursor ion stability, suggesting that changes to the number of mannose residues has practically no effect the information content of the resulting CID spectra when acquired at the same collision energies.

Conclusions

Measurement of precursor ion survival curves and 50% precursor ion survival energies was performed *via* low-energy beam-type CID for 30 protonated glycopeptide ions spanning four peptide sequences, four high mannose *N*-glycan compositions, and three charge states. The data acquired demonstrate that the precursor ion stabilities are heavily dependent upon charge state and peptide composition, as observed in previous studies. Contrastingly, the size and composition of the glycan moiety has a weak to negligible influence on the precursor ion stabilities, regardless of whether the available degrees of vibrational freedom are accounted for. It also appears that any minor differences in precursor ion survival are primarily due to the differing availability of vibrational degrees of freedom, and not related to any changes in the dissociation chemistry at hand. In paired spectra of $GlcNAc_2Man_5$ and $GlcNAc_2Man_8$ glycoforms, highly correlated spectra were observed when the peptide group, charge state, and collision energy were held constant. The fragments that were detected afforded highly concordant information on the composition and connectivity of the oligosaccharide group and the polypeptide chain, despite the fact that the same collision energy was used to probe the different high mannose glycoforms. The finding that glycan size and composition exerted only a minor influence over glycopeptide precursor ion stability and the information content of the corresponding CID spectra is a potentially simplifying factor for the acquisition of informative MS/MS data for N-linked glycopeptides. This introduces the possibility that many glycoforms of the same peptide could be optimally probed by CID under the same MS/MS conditions, thus removing one variable from a complex set of considerations where the fragmentation of glycopeptides is concerned. Indeed, the ability to obtain comparable structural information for closely related *N*-glycoforms without the need to modulate CID collision energy may prove to be a significant observation from the standpoint for automated, online glycoproteomic analyses. Overall, we believe that these findings have implications of considerable breadth for glycoproteomic analysis, as CID is, by a great margin, the most widely available MS/MS method. Future research in this area should include an investigation of whether these observations are generalizable to *N*-glycopeptides of different classes (*e.g.*, those harboring complex type and hybrid type glycans) and incorporating additional monosaccharides (*e.g.*, fucose and sialic acid residues).

Conflicts of interest

There are no conflicts to declare.

Acknowledgements

The authors wish to convey their sincere thanks to Venkata Kolli and Yuting Huang for helpful comments on a draft of the manuscript. This work was supported in part by funding from the National Science Foundation, Division of Chemistry, through the Chemical Measurement and Imaging Program (grant number 1507989). Support from the National Institutes of Health, National Institute for General Medical Sciences, is also acknowledged, including a Maximizing Investigators' Research Award (grant number R35GM128926), and a seed grant from the Nebraska Center for Integrated Biomolecular Communication (grant number P20GM113126).

References

1 A. Varki, *Glycobiology*, 1993, **3**, 97–130.
2 R. A. Dwek, *Chem. Rev.*, 1996, **96**, 683–720.

3 R. G. Spiro, *Glycobiology*, 2002, **12**, 43R–56R.
4 E. Weerapana and B. Imperiali, *Glycobiology*, 2006, **16**, 91R–101R.
5 K. Ohtsubo and J. D. Marth, *Cell*, 2006, **126**, 855–867.
6 H. J. An, S. R. Kronewitter, M. L. A. de Leoz and C. B. Lebrilla, *Curr. Opin. Chem. Biol.*, 2009, **13**, 601–607.
7 K. N. Schumacher and E. D. Dodds, *Glycoconjugate J.*, 2016, **33**, 377–385.
8 B. Adamczyk, T. Tharmalingam and P. M. Rudd, *Biochim. Biophys. Acta*, 2012, **1820**, 1347–1353.
9 M. N. Christiansen, J. Chik, L. Lee, M. Anugraham, J. L. Abrahams and N. H. Packer, *Proteomics*, 2014, **14**, 525–546.
10 S. R. Stowell, T. Ju and R. D. Cummings, *Annu. Rev. Pathol. Mech. Dis.*, 2015, **10**, 473–510.
11 E. Marklova and Z. Albahri, *Clin. Chim. Acta*, 2007, **385**, 6–20.
12 H. Schachter and H. H. Freeze, *Biochim. Biophys. Acta*, 2009, **1792**, 925–930.
13 L. Sturiale, R. Barone and D. Garozzo, *J. Inherited Metab. Dis.*, 2011, **34**, 891–899.
14 H. H. Freeze, *J. Biol. Chem.*, 2013, **288**, 6936–6945.
15 P. M. Rudd and R. A. Dwek, *Crit. Rev. Biochem. Mol. Biol.*, 1997, **32**, 1–100.
16 L. S. C. Kreisman and B. A. Cobb, *Glycobiology*, 2012, **22**, 1019–1030.
17 Y. Y. Zhao, M. Takahashi, J. G. Gu, E. Miyoshi, A. Matsumoto, S. Kitazume and N. Taniguchi, *Cancer Sci.*, 2008, **99**, 1304–1310.
18 G. W. Hart, C. Slawson, G. Ramirez-Correa and O. Lagerlof, *Annu. Rev. Biochem.*, 2011, **80**, 825–858.
19 W. Morelle, K. Canis, F. Chirat, V. Faid and J. C. Michalski, *Proteomics*, 2006, **6**, 3993–4015.
20 W. Morelle and J. C. Michalski, *Nat. Protoc.*, 2007, **2**, 1585–1602.
21 J. E. Schiel, *Anal. Bioanal. Chem.*, 2012, **404**, 1141–1149.
22 W. R. Alley Jr., B. F. Mann and M. V. Novotny, *Chem. Rev.*, 2013, **113**, 2668–2732.
23 M. V. Novotny and W. R. Alley Jr., *Curr. Opin. Chem. Biol.*, 2013, **17**, 832–840.
24 S. Gaunitz, G. Nagy, N. L. B. Pohl and M. V. Novotny, *Anal. Chem.*, 2017, **89**, 389–413.
25 D. S. Dalpathado and H. Desaire, *Analyst*, 2008, **133**, 731–738.
26 H. J. An, J. W. Froehlich and C. B. Lebrilla, *Curr. Opin. Chem. Biol.*, 2009, **13**, 421–426.
27 H. Desaire, *Mol. Cell. Proteomics*, 2013, **12**, 893–901.
28 V. Kolli, K. N. Schumacher and E. D. Dodds, *Bioanalysis*, 2015, **7**, 113–131.
29 H. Desaire and D. Hua, *Int. J. Mass Spectrom.*, 2009, **287**, 21–26.
30 J. W. Froehlich, E. D. Dodds, M. Wilhelm, O. Serang, J. A. Steen and R. S. Lee, *Mol. Cell. Proteomics*, 2013, **12**, 1017–1025.
31 M. Wuhrer, M. I. Catalina, A. M. Deelder and C. H. Hokke, *J. Chromatogr. B: Anal. Technol. Biomed. Life Sci.*, 2007, **849**, 115–128.
32 E. D. Dodds, *Mass Spectrom. Rev.*, 2012, **31**, 666–682.
33 R. A. Zubarev, A. R. Zubarev and M. M. Savitski, *J. Am. Soc. Mass Spectrom.*, 2008, **19**, 753–761.
34 J. J. Coon, *Anal. Chem.*, 2009, **81**, 3208–3215.
35 S. A. McLuckey and M. Mentivona, *J. Am. Soc. Mass Spectrom.*, 2011, **22**, 3–12.
36 D. Rathore, F. Aboufazeli, Y. Huang, V. Kolli, G. S. Fernando and E. D. Dodds, *Encycl. Anal. Chem.*, 2015, 1–26.
37 M. Tajiri, M. Kadoya and Y. Wada, *J. Proteome Res.*, 2009, **8**, 688–693.
38 K. Vekey, O. Ozohanics, E. Toth, A. Jeko, A. Revesz, J. Krenyacz and L. Drahos, *Int. J. Mass Spectrom.*, 2013, **345–347**, 71–79.
39 E. Mirgorodskaya, P. Roepstorff and R. A. Zubarev, *Anal. Chem.*, 1999, **71**, 4431–4436.
40 K. Hakansson, H. J. Cooper, M. R. Emmett, C. E. Costello, A. G. Marshall and C. L. Nilsson, *Anal. Chem.*, 2001, **73**, 4530–4536.
41 N. Manri, H. Satake, A. Kaneko, A. Hirabayashi, T. Baba and T. Sakamoto, *Anal. Chem.*, 2013, **85**, 2056–2063.
42 J. M. Hogan, S. J. Pitteri, P. A. Chrisman and S. A. McLuckey, *J. Proteome Res.*, 2005, **4**, 628–632.
43 M. I. Catalina, C. A. Koeleman, A. M. Deelder and M. Wuhrer, *Rapid Commun. Mass Spectrom.*, 2007, **21**, 1053–1061.
44 J. P. Williams, S. Pringle, K. Richardson, L. Gethings, J. P. C. Vissers, M. De Cecco, S. Houel, A. B. Chakraborty, Y. Q. Yu, W. Chen and J. M. Brown, *Rapid Commun. Mass Spectrom.*, 2013, **27**, 2383–2390.
45 J. T. Adamson and K. Hakansson, *J. Proteome Res.*, 2006, **5**, 493–501.
46 R. R. Seipert, E. D. Dodds, B. H. Clowers, S. M. Beecroft, J. B. German and C. B. Lebrilla, *Anal. Chem.*, 2008, **80**, 3684–3692.
47 R. R. Seipert, E. D. Dodds and C. B. Lebrilla, *J. Proteome Res.*, 2009, **8**, 493–501.
48 L. Zhang and J. P. Reilly, *J. Proteome Res.*, 2008, **8**, 734–742.
49 J. A. Madsen, B. J. Ko, H. Xu, J. A. Iwashkiw, S. A. Robotham, J. B. Shaw, M. F. Feldman and J. S. Brodbelt, *Anal. Chem.*, 2013, **85**, 9253–9261.
50 B. J. Ko and J. S. Brodbelt, *Int. J. Mass Spectrom.*, 2015, **377**, 385–392.
51 H. Han, Y. Xia, M. Yang and S. A. McLuckey, *Anal. Chem.*, 2008, **80**, 3492–3497.
52 I. Perdivara, R. Petrovich, B. Allinquant, L. J. Deterding, K. B. Tomer and M. Przybylski, *J. Proteome Res.*, 2009, **8**, 631–642.
53 Z. Darula, R. J. Chalkley, P. Baker, A. L. Burlingame and K. F. Medzihradszky, *Eur. J. Mass Spectrom.*, 2010, **16**, 421–428.
54 C. Singh, C. G. Zampronio, A. J. Creese and H. J. Cooper, *J. Proteome Res.*, 2012, **11**, 4517–4525.
55 V. Kolli, K. N. Schumacher and E. D. Dodds, *Analyst*, 2017, **142**, 4691–4702.
56 W. R. Alley Jr., Y. Mechref and M. V. Novotny, *Rapid Commun. Mass Spectrom.*, 2009, **23**, 161–170.

57 Z. Zhu, D. Hua, D. F. Clark, E. P. Go and H. Desaire, *Anal. Chem.*, 2013, **85**, 5023–5032.
58 V. Kolli and E. D. Dodds, *Analyst*, 2014, **139**, 2144–2153.
59 V. Kolli, H. A. Roth, G. De La Cruz, G. S. Fernando and E. D. Dodds, *Anal. Chim. Acta*, 2015, **896**, 85–92.
60 O. Krokhin, W. Ens, K. G. Standing, J. Wilkins and H. Perreault, *Rapid Commun. Mass Spectrom.*, 2004, **18**, 2020–2030.
61 N. V. Bykova, C. Rampitsch, O. Krokhin, K. G. Standing and W. Ens, *Anal. Chem.*, 2006, **78**, 1093–1103.
62 C. W. Damen, W. Chen, A. B. Chakraborty, M. van Oosterhout, J. R. Mazzeo, J. C. Gebler, J. H. Schellens, H. Rosing and J. H. Beijnen, *J. Am. Soc. Mass Spectrom.*, 2009, **20**, 2021–2033.
63 Z. M. Segu and Y. Mechref, *Rapid Commun. Mass Spectrom.*, 2010, **24**, 1217–1225.
64 N. E. Scott, B. L. Parker, A. M. Connolly, J. Paulech, A. V. G. Edwards, B. Crossett, L. Falconer, D. Kolarich, S. P. Djordjevic, P. Hojrup, N. H. Packer, M. R. Larsen and S. J. Cordwell, *Mol. Cell. Proteomics*, 2011, **10**, 1–18.
65 Q. Cao, X. Zhao, Q. Zhao, X. Lv, C. Ma, X. Li, Y. Zhao, B. Peng, W. Ying and X. Qian, *Anal. Chem.*, 2014, **86**, 6804–6811.
66 H. Hinneburg, K. Stavenhagen, U. Schweiger-Hufnagel, S. Pengelley, W. Jabs, P. H. Seeberger, D. V. Silva, M. Wuhrer and D. Kolarich, *J. Am. Soc. Mass Spectrom.*, 2016, **27**, 507–519.
67 J. Nilsson, *Glycoconjugate J.*, 2016, **33**, 261–272.
68 A. R. Dongre, J. L. Jones, A. Somogyi and V. H. Wysocki, *J. Am. Chem. Soc.*, 1996, **118**, 8365–8374.
69 V. H. Wysocki, G. Tsaprailis, L. L. Smith and L. A. Breci, *J. Mass Spectrom.*, 2000, **35**, 1399–1406.
70 F. Aboufazeli, V. Kolli and E. D. Dodds, *J. Am. Soc. Mass Spectrom.*, 2015, **26**, 587–595.
71 B. Domon and C. E. Costello, *Glycoconjugate J.*, 1988, **5**, 397–409.
72 P. Roepstorff and J. Fohlman, *Biomed. Mass Spectrom.*, 1984, **11**, 601.
73 A. Varki, R. D. Cummings, J. D. Esko, H. H. Freeze, P. Stanley, J. D. Marth, C. R. Bertozzi, G. W. Hart and M. E. Etzler, *Proteomics*, 2009, **9**, 5398–5399.
74 A. Varki, R. D. Cummings, M. Aebi, N. H. Packer, P. H. Seeberger, J. D. Esko, P. Stanley, G. Hart, A. Darvill, T. Kinoshita, J. J. Prestegard, R. L. Schnaar, H. H. Freeze, J. D. Marth, C. R. Bertozzi, M. E. Etzler, M. Frank, J. F. G. Vliegenthart, T. Lütteke, S. Perez, E. Bolton, P. Rudd, J. Paulson, M. Kanehisa, P. Toukach, K. F. Aoki-Kinoshita, A. Dell, H. Narimatsu, W. York, N. Taniguchi and S. Kornfeld, *Glycobiology*, 2015, **25**, 1323–1324.
75 P. Juhasz and S. A. Martin, *Int. J. Mass Spectrom.*, 1997, **169**, 217–230.
76 H. J. An, T. R. Peavy, J. L. Hedrick and C. B. Lebrilla, *Anal. Chem.*, 2003, **75**, 5628–5637.
77 B. H. Clowers, E. D. Dodds, R. R. Seipert and C. B. Lebrilla, *J. Proteome Res.*, 2007, **6**, 4032–4040.
78 E. D. Dodds, R. R. Seipert, B. H. Clowers, J. B. German and C. B. Lebrilla, *J. Proteome Res.*, 2009, **8**, 502–512.
79 B. Paizs and S. Suhai, *Mass Spectrom. Rev.*, 2005, **24**, 508–548.
80 S. Indelicato, D. Bongiorno, S. Indelicato, L. Drahos, V. Turco Liveri, L. Turiak, K. Vekey and L. Ceraulo, *J. Mass Spectrom.*, 2013, **48**, 379–383.
81 A. Memboeuf, A. Nasioudis, S. Indelicato, F. Pollreisz, A. Kuki, S. Keki, O. F. van den Brink, K. Vekey and L. Drahos, *Anal. Chem.*, 2010, **82**, 2294–2302.